Fluorescence lifetime dynamics of enhanced green fluorescent protein in protein aggregates with expanded polyglutamine

Vladimir Ghukasyan
Chih-Chun Hsu
National Yang-Ming University
Institute of Biophotonics
155 Li-Nong Street Section 2
Taipei 112, Taiwan

Chia-Rung Liu
National Yang-Ming University
Institute of Biochemistry and Molecular Biology
155 Li-Nong Street Section 2
Taipei 112, Taiwan

Fu-Jen Kao
National Yang-Ming University
Institute of Biophotonics
155 Li-Nong Street Section 2
Taipei 112, Taiwan

Tzu-Hao Cheng
National Yang-Ming University
Institute of Biochemistry and Molecular Biology
155 Li-Nong Street Section 2
Taipei 112, Taiwan

Abstract. Protein aggregation is one of the characteristic steps in a number of neurodegenerative diseases eventually leading to neuronal death and thorough study of aggregation is required for the development of effective therapy. We apply fluorescence lifetime imaging for the characterization of the fluorescence dynamics of the enhanced green fluorescent protein (eGFP) in fusion with the polyQ—expanded polyglutamine stretch. At the expansion of polyQ above 39 residues, it has an inherent propensity to form amyloid-like fibrils and aggregates, and is responsible for Huntington's disease. The results of the experiments show that expression of the eGFP in fusion with the 97Q protein leads to the decrease of the eGFP fluorescence lifetime by ~300 ps. This phenomenon does not appear in Hsp104-deficient cells, where the aggregation in polyQ is prevented. We demonstrate that the lifetime decrease observed is related to the aggregation per se and discuss the possible role of refractive index and homo-FRET in these dynamics. [DOI: 10.1117/1.3290821]

Keywords: enhanced green fluorescent protein; aggregation; polyglutamine; fluorescence lifetime imaging; Förster resonance energy transfer; fluorescence anisotropy imaging; refractive index; homo-FRET.

Paper 09196PR received May 15, 2009; revised manuscript received Oct. 19, 2009; accepted for publication Nov. 16, 2009; published online Jan. 15, 2010.

1 Introduction

Failure of some proteins to adopt or maintain their native conformational state may result in a number of disorders, grouped under the name of protein misfolding diseases. These misfoldings usually lead to the conversion of detergent-soluble forms into amyloid fibrils—highly organized and generally intractable protein aggregates enriched in β-sheet structure.[1] One of the causes of such aggregation is a mutation in certain genes, which result in the expanded repeats of CAG trinucleotide, encoding glutamine. The abnormal expansion of the polyglutamine tract (polyQ) leads to misfolding, aggregation, inclusion body formation, and eventual neuronal cell death in nine inherited neurodegenerative disorders, including Huntington's disease, dentatorubral pallidoluysian atrophy, spinal and bulbar muscular atrophy, and several types of spinocerebellar ataxia.[2–5] Efficiency of aggregation increases with the length of polyQ track in yeast and mammalian cells, whereby polypeptides with less than 39 glutamine residues fail to aggregate at all.[6–8] Consistent with this notion, in Huntington's disease polyQ repeats are expanded from normal 8 to 25 to more than 39 at the *N*-terminus of the huntingtin protein.[9,10]

Despite the fact that pathogenicity of the polyQ aggregation has been known for some time, there is poor evidence in misfolding diseases management and development of effective therapies requires better understanding of aggregates formation.[11] Several fluorescence spectroscopy techniques have been applied for this purpose, such as fluorescence microscopy,[12] fluorescence correlation spectroscopy,[13,14] and Förster resonance energy transfer (FRET) imaging microscopy. One of the most popular techniques, FRET has been applied[15–20] to study the involvement of other proteins in the aggregates formation and discrimination between mono- and oligomers of polyQ (also reviewed in Ref. 21). The technique is based on the nonradiative energy transfer from the excited donor molecule to another fluorescent moiety, the acceptor. For the transfer to happen, the molecules must be in close proximity (within the range of 2 to 10 nm), which makes FRET an ideal technique to study interactions between molecules.[22]

The fluorescence spectroscopy techniques are based on the labeling of the protein(s) of interest with further monitoring of the fluorescence signal properties and distribution. However, possible complex interactions between many fluorophores in close proximity, as well as the change of their microenviron-

Address all correspondence to: Tsu-Hao Cheng, National Yang-Ming University, Institute of Biochemistry and Molecular Biology, 155 Li-Nong Street Section 2, Taipei 112, Taiwan. Tel: 886-2-28267129; Fax: 886-2-28264843; E-mail: thcheng@ym.edu.tw; or Fu-Jen Kao, National Yang-Ming University, Institute of Biophotonics, 155 Li-Nong Street Section 2, Taipei 112, Taiwan; Tel: 886-2-28267336; Fax: 886-2-28235460; E-mail: fjkao@ym.edu.tw

1083-3668/2010/15(1)/016008/11/$25.00 © 2010 SPIE

ment in aggregates, can influence the resulting photophysical properties and thorough characterization of such changes is required for the correct interpretation of the data.

In this work, we have examined the changes caused by aggregation to the average time that fluorophore molecules spend on the excited state levels on photon absorption and prior to the relaxation to the ground state—the fluorescence lifetime. At this, the relaxation through photon emission competes with a number of alternative pathways of excessive energy release given that they happen in the time scale comparable with the fluorescence lifetime. Among these are protonation, electron transfer, collisional quenching, and nonradiative energy transfer.[23] In FRET, for example, the energy transfer from donor to acceptor creates an additional pathway for the depletion of the donor's excited state levels, thus shortening the radiative decay and correspondingly lowering the fluorescence lifetime values.[23] This sensitivity of the technique made it possible to probe the environment of proteins in cells in terms of its refractive index,[24] pH (Ref. 25), and ion concentration,[26] to perform dynamic imaging of the redox state,[27] to follow signaling and trafficking,[28] and to monitor protein localization and interactions.[29] Fluorescence lifetime microscopy (FLIM) can also be applied for the monitoring of conformation, especially[30] in combination with FRET. Previously, FLIM has also been applied in the studies of misfolding proteins.[31–33]

One of the most applied fluorescent markers, the green fluorescent protein (GFP) is a 238-amino-acid-long polypeptide, isolated from the jellyfish *Aequorea victoria*.[34,35] The chromophore of the wild-type GFP is a *p*-hydroxybenzylidene-imidazolidinone derivative formed by an autocatalytic posttranslational cyclization and oxidation of Ser-65, Tyr-66, and Gly-67 (Ref. 36). Located in the middle of a rigid 11-stranded barrel, the chromophore is rigidly embedded in the protein matrix and thus is isolated from the bulk solvent. The barrel shielding makes the GFP almost completely insensitive to the solvent polarity, ionic strength, and viscosity. The convenience of GFP comes from the autocatalytical nature of its chromophore synthesis, so that the expression of the fusion gene of GFP and a protein of interest in a cell requires no additional cofactors, thus minimizing the impact on the cell environment and making the operation easy.

Despite the tremendous potential of the wild-type GFP, it has a few deficiencies. The formation of dimers in some conditions complicates the results interpretation and might also affect the labeled protein functionality.[37] Moreover, from the two absorption peaks of wild-type GFP, the one at 396 nm has higher amplitude at lower photostability as compared to the more stable peak at 475 nm. A number of mutants with improved fluorescence characteristics of the GFP have been developed. A popular variant enhanced GFP (eGFP) holds a double mutation of Ser65→Thr and Phe64→Leu with the former shifting the absorption spectrum to the blue range and increasing brightness, and the latter supporting protein folding at high temperatures.[38] Having the same structure with the GFP, this enhanced variant of the fluorescent protein is, however, sensitive to the acidic environment[25] (pH$<$4.0). This variant has been demonstrated as a well-expressed monomer and gained wide acceptance.[39]

We examined the changes in the fluorescence lifetime dynamics of eGFP fused to 97Q protein (97Q-eGFP) by means of FLIM in model yeast cells and found that the lifetime of the fluorophore is decreasing on aggregation. To properly assess the influence of the aggregation of the labeled 97Q on the fluorescence lifetime of eGFP, we identified other possible causes for the radiative decay dynamics. We assessed the contribution of the pH level, direct nonradiative transfer to fluorescent metabolites, and level of cellular autofluorescence and environmental changes caused by physiological cells conditions on the dynamics of the eGFP fluorescence lifetime. We also investigated existence of FRET between eGFP molecules in 97Q aggregates. The possible influence of such nonradiative transfer and refractive index on the phenomenon observed is discussed.

2 Materials and Methods

2.1 *Plasmid and Yeast Strain Constructions*

The pYES2-97Q-eGFP plasmid was based on the pYES2-103Q-eGFP, kindly provided by Sherman, was described in Ref. 40. A reduction of six glutamine residues in the expected repeat region was found on conducting the DNA sequencing of the plasmid, hence the new construct pYES2-97Q-eGFP, used throughout all the subsequent experiments. The pYES2-eGFP plasmid construct was derived from pYES2-97Q-eGFP by deleting the DNA region encoding 97Q. With polymerase chain reaction (PCR), the DNA fragment covering Gal1 promoter and Flag tag of pYES2-97Q-eGFP was amplified using EcoRI-Gal-97Q-ADE2 5′ primer: GGAATTCCGCTTAATGGGGCGCTACAG and Gal-Flag-SmaI 3′ primer: TGCCTCCCGGGTTTGAGGGACTCGAAGGCCTTC. The PCR product was digested with *Kpn* I and *Sma* I, and then replaced the *Kpn* I-*Sma* I fragment of pYES-97Q-eGFP to create pYES2-eGFP. Each of the two plasmids (pYES2-97Q-eGFP and pYES2-eGFP) was transformed into *Saccharomyces cerevisiae* W303-1a (*MATa ade2-1 trp1-1 ura3-1 leu2-3,112 his3-11,15 can1-100*).

To make the *hsp*104 knock-out strain (hsp104Δ), the entire coding sequence of *HSP*104 gene was replaced with a *KanMX* gene by the one-step gene disruption method.[41] The targeting DNA was amplified by PCR (HSP104-KAN 5′ primer: ATGAACGACCAAACGCAATTTACAGAAAGGGCTCTAACGATTTTGACGTTAGCTTGCCTCGTCCCCGCCGG and HSP104-KAN 3′ primer: TTAATCTAGGTCATCATCAATTTCCATACTGTCCTCATTATCGTCATCACTCGACACTGGATGGCGGCGTTAG, plasmid pUG6 as a template) and transformed into *S. cerevisiae* W303-1a. Transformants were selected on YPDA/G418 plates and the hsp104Δ strain was confirmed by genomic PCR.

2.2 *Development of Ade2-Proficient Strains*

Both wild type W303-1a (wt) and hsp104Δ cells had characteristic adenine synthesis blockade caused by Ade2 deficiency, which led to the accumulation of intermediates, absorbing in the range of eGFP's fluorescence. To check the nonradiative transfer from eGFP, the adenine metabolism was restored by turning the cells into Ade2-proficient by introducing the pRS424-Flag-ADE2 plasmid construct.

For this purpose, the *ADE2* gene was amplified using BamHI-Flag-ADE2 5′ primer: CGGGATCCATGGACTACAAGGACGACGATGACAAGCTGGCGACCCTGGAAAAGCTGGATTCTAGAACAGTTGGTATA and NheI-ADE2-

HA 3′ primer: CTAGCTAGCTTAGATGATGGCGTAGTCGGGCA CGTCGTAGGGGT AATGGCGGCCGCCC TTGTTTTCTAGATAAGCTTC in a PCR reaction. Following *BamH* I and *Nhe* I digestion, the resulting fragment was ligated into the pYES2 plasmid, which was linearized by *BamH* I and *Xba* I to create pYES2-Flag-ADE2. Using this plasmid as a template, the Flag-tagged *ADE2* gene as well as the upstream GAL1 promoter was subsequently subcloned into pRS424 plasmid vector to generate pRS424-Flag-ADE2.

2.3 *Cell Growth Assay*

For the assessment of 97Q cytotoxicity, a cell growth assay was carried out. Cells were precultured in synthetic dropout media containing 2% dextrose at 30 °C. An appropriate amount of the cell suspension was then transferred to a fresh medium that contained 2% galactose as the sole carbon source to induce the expression of eGFP or 97Q-eGFP. After 12 h culturing, the cell density usually reached $OD_{600}=2$ and the cells were mounted on an agarose slide to measure the cellular distribution of eGFP and its fluorescence lifetime. The influence of Ade2 deficiency was eliminated by reintroducing the expression of the *ADE2* gene from pRS424-Flag-ADE2 in these cells.

2.4 *Imaging System Setup*

The measurements were conducted on the time-resolved two-photon fluorescence spectroscopy system, built around the modified laser-scanning microscope (IX71, Olympus Corp.). The sample was excited at 860 nm by a mode-locked femtosecond linearly polarized Ti:sapphire Mira F-900 laser (Coherent, Inc.), operated in two-photon mode at a 76-MHz frequency. The wavelength choice is explained with the lowest autofluorescence level detected at this excitation band. The intensity of the laser power was kept within 3.5 mW above the objective. The beam was fed into the scanning unit (FV300, Olympus Corp.) and scanned across the sample at the speed controlled externally by a function generator (AFG310, Tektronix Inc.). The 60×1.4 numerical aperture (NA) PlanApochromat lens (Olympus Corp.) focused the beam at the cell samples and collected the fluorescence photons, which were delivered in a nondescanned mode to the photomultiplier tube (H7422-P40, Hamamatsu Photonics K.K.) mounted at the backport of the microscope. A 520 ± 17.5-nm filter (FF01-520/35-25, Semrock) was installed along with the IR cut-off filter (Edmund Optics, Inc.) in the detection channel for the selective acquisition of eGFP fluorescence. Signal synchronization and building of the time-resolved data matrix were conducted by the SPC-830 time-correlated single photon counting (TCSPC) board[42] (Becker&Hickl GmbH). All the images were taken at 256×256 pixels resolution with the acquisition time varying in the range of 200 to 600 s. No significant change of the photon count rate was detected during the measurements.

For the anisotropy imaging, the horizontal polarization of the laser was utilized without additional polarizers in the excitation pathway. A Glan-laser polarizer (GL10, Thorlabs Ltd.) with a coating wavelength range of 300 to 600 nm was installed in the detection pathway. The measurements in the polarization plane parallel ($I_{\parallel}$) and perpendicular ($I_{\perp}$) to that of the laser was taken successively by manually rotating the mounted polarizer. To decrease the depolarization caused by the optics, an objective of lower NA (0.9, 40×) was used for anisotropy imaging. Photon distribution was registered with the TCSPC board with the same settings as for the fluorescence lifetime imaging.

2.5 *Data Analysis*

Data analysis via model function fitting, instrument response function (IRF) deconvolution, and color coding were conducted with the commercially available SPCImage software package (v. 2.9, Becker&Hickl, GmbH). A mathematical model was fitted to the experimental data by iterative non-least-squares reconvolution:

$$I_c(t)=\int_{-\infty}^{\infty} I_{\mathrm{instr}}(t)\left\{I_0+\sum_{i=1}^{n} a_i[\exp(-t/\tau_i)]\right\}\mathrm{d}t, \qquad (1)$$

where I_{instr} is the instrument response, I_0 is the baseline offset, and $a_i[\exp(-t/\tau_i)]$ are the main components of the fluorescence decay. The a_i preexponential coefficients have relative amplitudes and demonstrate the correlation between components fractions populations, τ_i are the lifetimes of all the components to the decay (in case of multiexponential one). The IRF of the setup was measured from the second harmonic generated by the periodically poled lithium niobate (PPLN) crystal. The measured full width at half maximum of the IRF was ~320 ps and represented the IRF of the whole system.

The quality of fitting was judged by the residual function distribution and reduced goodness-of-fit parameter calculated by the equation

$$\chi_R^2=\left\{\sum_{k=1}^{n}[I_e(t)-I_c(t)]^2/I_e(t)\right\}\Big/(n-p), \qquad (2)$$

where $I_e(t)$ is the actual experimental data, $I_c(t)$ is the calculated decay as already described, n is the number of the data (time) points (256 time channels for the given work), and p is the number of model parameters. The χ_R^2 was minimized by the Levenberg-Marquardt search algorithm.

To remove the background and signal from dead cells with high autofluorescence levels either the regions of interest were marked so that only the pixels inside the region were used to generate the lifetime distribution histogram, or a threshold parameter was used. A pixel binning factor of 2 was applied in our analysis, so that a signal from 25 adjacent pixels was used to derive a single decay curve for further fitting. All the pixels within the specified region and with the number of the photon counts higher than the threshold defined were then analyzed and pixel frequency-weighted lifetime distribution histograms were built.

Fluorescence anisotropy data were analyzed by the custom developed program for MATLAB software package (The Mathworks, Inc.). The program parsed the TCSPC-generated files of the $I_{\parallel}$ and perpendicular $I_{\perp}$ measurements, fetched the photons distribution data and summed together the number of the photons for all 256 time channels in each pixel. The numbers thus obtained were then used for the calculation of steady state anisotropy:

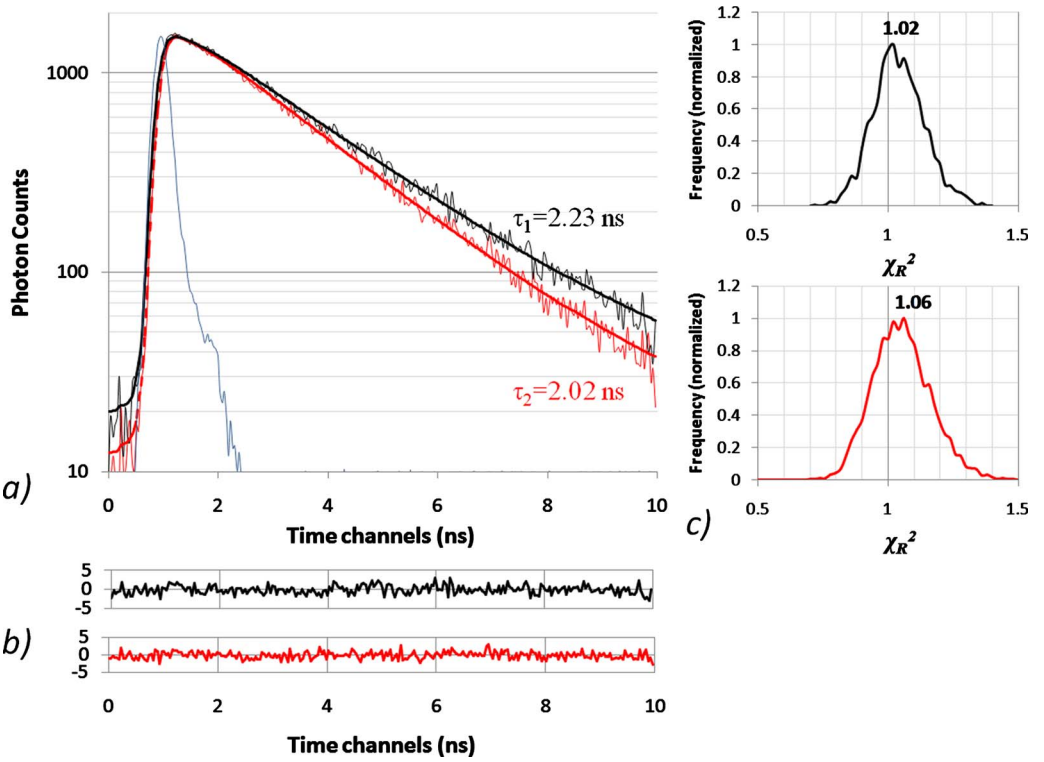

Fig. 1 Representative fluorescence lifetime decays and histograms of the goodness of fit measured from the eGFP(wt) (black) and 97Q-eGFP(wt) (red). The decay data (a) clearly demonstrates different lifetimes for both samples. The IRF is represented in blue. Both decays could be successfully fitted with single-exponential model, as seen from the residual functions (b) and distribution of the goodness-of-fit histogram obtained from the whole image (c). (Color online only.)

$$r = \frac{I_{\parallel} - GI_{\perp}}{I_{\parallel} + 2GI_{\perp}}, \tag{3}$$

where G is the correction factor applied to account for the differences in the sensitivity of the detection optics for vertically and horizontally polarized light. For our case, the value of 1 was applied since no monochromator was used and both polarization plane signals were detected with the same channel.

Statistical processing of the data was carried out with the single-factor analysis of variance (ANOVA). The similarity and diversity of the data sets were conducted by comparing the peak values of the fluorescence lifetime histograms recorded from the images.

2.6 *Colocalization Imaging*

The wt and hsp104Δ cells with the expressed 97Q-eGFP were grown in an adenine-restricted medium (adenine final concentration of 4 mg/L) for 24 h, resulting in red ade2 dye overproduced and accumulated in vacuole.[43] The cells were mounted on the agarose pad of a single-cavity slide and visualized by the fluorescence microscope Axioskop 2 (Carl Zeiss Microimaging Inc.) with a 100× oil immersion objective. The differential interference contrast (DIC) images were taken for phase contrast. eGFP was excited at 470 to 500 nm, and ade2 dye was excited at 525 to 550 nm.

3 Results

3.1 *eGFP Fluorescence Lifetime Decreases in 97Q Aggregates*

To study the dynamics of the eGFP fluorescence lifetime in aggregates, the fluorophore was lagated with 97Q protein with a linker of seven aminoacids. The fluorescence decays recorded for eGFP, both expressed solely and fused to 97Q protein, were well fitted with a single-exponential model, as judged by the distribution of residual functions and goodness of fit (Fig. 1). Although for the 97Q-eGFP expressed in wt cells, further denoted as 97Q-eGFP(wt), the goodness of fit appeared slightly increased as compared to the free eGFP in same cells [eGFP(wt)], application of a double-exponential decay model did not improve the fitting quality. The difference between the decays was well distinguishable with the one measured from the 97Q-eGFP(wt) having steeper slope.

The change in the eGFP lifetime behavior at fusion to the 97Q is well illustrated with the distribution of the averaged histograms, collected from the series of images [Fig. 2(d)]. The histogram of eGFP(wt) stretches from ~2 to ~2.4 ns with the peak value mean of 2.29 ± 0.03 ns. Ligation of eGFP to 97Q resulted in the shift of the histogram to the shorter values region. It appears slightly wider with the stretch from ~1.7 to ~2.4 ns and the maximum mean of 2 ± 0.06 ns. The two histograms obtained are well separated and the peak value data set distribution is significantly different ($P < e-22$).

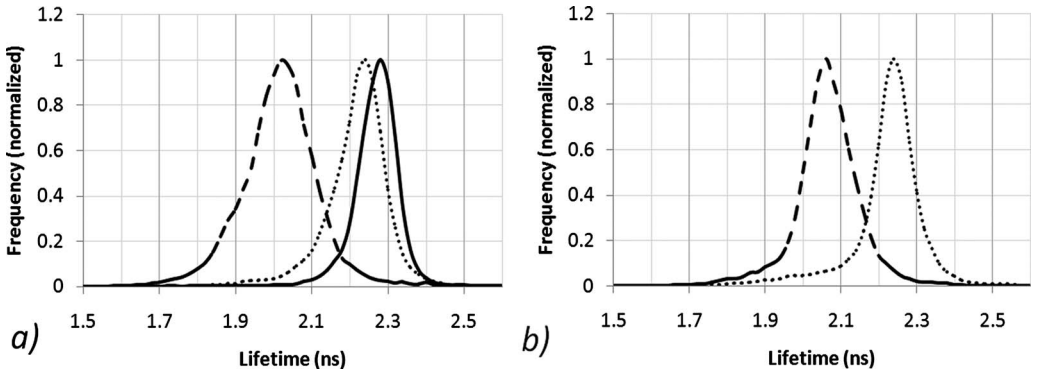

Fig. 2 Averaged fluorescence lifetime histograms, measured from the eGFP alone and fused with 97Q. (a) The histogram obtained from the 97Q-eGFP(wt) (dashed line) is significantly shifted to the shorter values range as compared to the eGFP(wt) (solid line). Prevention of aggregation through the expression of 97Q-eGFP in hsp 104Δ cells resulted in the histogram shift back toward the native eGFP values (dotted line). (b) The same dynamics for the 97Q-eGFP lifetime is observed for the Ade2-proficient cells: shortening for 97Q-eGFP(wt Ade2) (dashed line) and restoration of the eGFP-original lifetime for 97Q-eGFP(hsp 104Δ Ade2) (dotted line).

The eGFP(wt) and 97Q-eGFP(wt) also exhibited different distribution patterns in yeast cells (Fig. 3). Free eGFP had a diffused distribution with the exception of the vacuole, where little to no signal was detected [Fig. 3(a)]. In contrast to that, the 97Q-eGFP exhibited grain- and cloudlike patterns, indicative of polyQ tract aggregation [Fig. 3(b)]. With the given color coding it is evident that the aggregates exhibit shorter lifetime than the surrounding.

To reveal the role of the aggregation in the lifetime dynamics observed, the 97Q-eGFP was expressed in the hsp104Δ strain, where the 97Q aggregation was prevented [hereinafter referred to as 97Q-eGFP(hsp104Δ)]. Intracellular protein aggregation is a complex process involving microtubule-mediated protein transport to the centrosome with further formation of the aggresomes, and regulated by chaperones and ubiquitin-proteasome degradation pathway components.[44–47] Among major factors involved in this process are heat shock proteins, which restore native conformation and support proper interaction of proteins aggregated at high temperature or as a result of environmental stress. In particular, overexpression of heat shock proteins Hsp70 and Hsp40 inhibits the formation of large detergent-soluble inclusion bodies, leading to the conversion of the aggregates into soluble forms.[48] However, for Hsp104, an opposite effect was demonstrated: under a normal growth condition, this protein can assist the formation of nonpathological aggregates, prions, and is essential for polyQ protein aggregation in yeast cells. In the absence of this chaperone, aggregation of prions and polyQ is prevented and these proteins become soluble.[8,40,49,50]

At aggregation prevention, the averaged lifetime histogram appeared narrower than that for the 97Q-eGFP(wt), and shifted back toward the lifetime values of eGFP(wt) with the peak mean of 2.23 ± 0.03 [Fig. 2(a)]. Similar to free eGFP, the 97Q-eGFP(hsp104Δ) appeared evenly distributed in the cytoplasm of cells [Fig. 3(c)], indicative of the lack of aggregation.

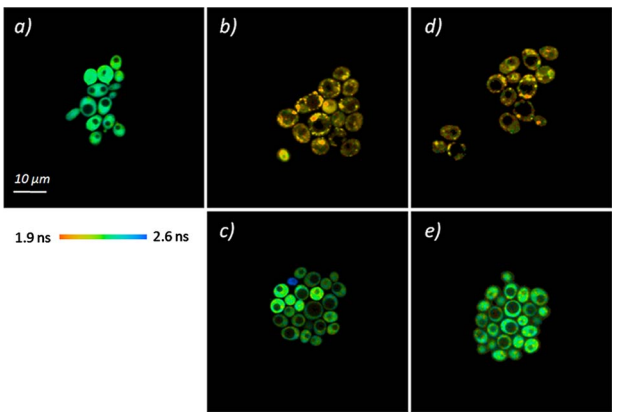

Fig. 3 Color-coded images of fluorescence lifetime distribution of (a) eGFP(wt), (b) 97Q-eGFP(wt), (c) 97Q-eGFP(hsp 104Δ), (d) 97Q-eGFP(wt Ade2), and (e) 97Q-eGFP(hsp 104Δ Ade2). (Color online only.)

3.2 *Red Metabolites: Influence of Hetero-FRET and pH*

The ade2 mutation, characteristic for the W303-1a strain, used in the experiments, is known to block adenine synthesis in cells and lead to the accumulation of intermediate metabolite 4-aminoimidazole ribotide. This colorless compound is synthesized in cytosol with further concentration of its derivatives in the vacuole, where it undergoes polymerization and oxidation, producing a red color.[51] The aminoimidazole and its derivatives were demonstrated in previous works to absorb at the wavelengths range of ~490 to 540 nm. Therefore, there was a possibility of direct nonradiative energy transfer from eGFP, given the overlapping of its emission and absorption spectra of these metabolites.[52] This may have caused the decrease of the eGFP lifetime as a donor.[29]

To examine the possibility of this energy transfer, we conducted control measurements with restored adenine metabolism by expressing Ade2 protein in W303-1a cells. The fluorescence lifetime of 97Q-eGFP in Ade2-proficient cells, hereinafter denoted as 97Q-eGFP(Ade2), exhibited peak value of 2.07 ± 0.02 ns, which appeared statistically identical to that of 97Q-eGFP(wt) with $P = 0.02$ [Fig. 2(b), Table 3 in Sec. 4]. Similar to that, the fluorescence lifetime value of 2.24 ± 0.02 ns obtained for the 97Q-eGFP in Ade2-proficient

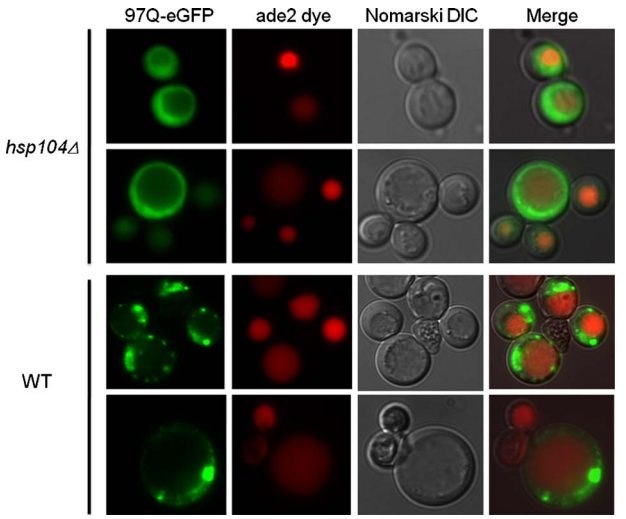

Fig. 4 Fluorescence intensity and differential contrast images of cells (wt and hsp 104Δ) expressing 97Q-eGFP. The vacuole was marked with the red fluorescent adenine metabolite, ade2 dye. The images clearly show lack of the green eGFP signal from the vacuole. (Color online only.)

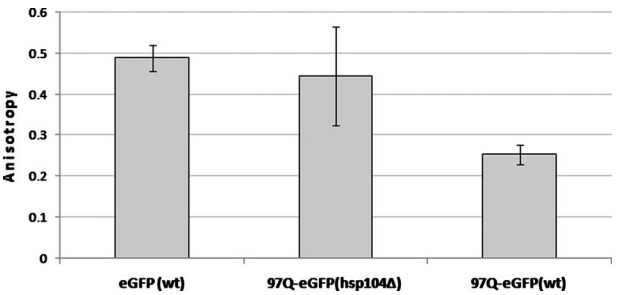

Fig. 5 Steady state anisotropy values for the controls [eGFP(wt) and 97Q-eGFP(hsp 104Δ)] and 97Q-eGFP aggregates in wt cells. High values of the steady state anisotropy for the control samples is a result of a slow rotation of the eGFP and nonaggregated fusion protein 97Q-eGFP. The lowest anisotropy value for the aggregated 97Q-eGFP in wt cells is caused by the FRET depolarization. Same phenomenon also causes somewhat lower values of the 97Q-eGFP(hsp 104Δ) and a larger standard deviation, since the prevention of aggregation in these samples has limited efficiency, which leads to low anisotropy values in some of the measurements.

hsp104Δ cells [97Q-eGFP(hsp104ΔAde2)] was indistinguishable from the results recorded form 97Q-eGFP (hsp104Δ) ($P=0.97$). The similarity applies also to the spatial distribution of the 97Q-eGFP in Ade2-proficent cells: grains with shorter fluorescence lifetime in wt cells [Fig. 3(d)], and evenly distributed pattern of longer lifetime for 97Q-eGFP in the absence of the Hsp104 chaperone [Fig. 3(e)].

The red ade2 pigment was also utilized in this study to investigate the influence of low pH on the eGFP lifetime values. Misfolded and aggregated proteins can hamper cellular function, and these proteins normally are degraded by lysosomes or proteasomes.[53] In yeast cells, the degradation occurs in vacuoles—organelles with acidic lumen,[54] which may shorten the eGFP lifetime. To investigate the contribution of pH level to the fluorescence lifetime dynamics observed, we checked the presence of eGFP in vacuole by colocalization experiments. The cells were grown in adenine restriction medium to mark the vacuole with the ade2 red pigment. The results, presented on Fig. 4, clearly show no overlapping of the eGFP signal with the red color of ade2, originating from the vacuole.

3.3 *Homo-FRET in Aggregates*

The resonance energy transfer can occur also between the molecules of the same fluorophore given that there is overlap between emission and absorption of the fluorescent species. Unlike FRET between different molecules, energy transfer between like molecules (homo-FRET) is typically not manifested in changes of fluorescence lifetime or intensity.[23] Recent works, however, have demonstrated that in some cases aggregation of fluorophores can still affect the rate of excited state levels depletion hence contributing to its fluorescence lifetime shortening.[55,56]

Homo-FRET is usually observed with fluorescence anisotropy imaging microscopy.[57–59] On excitation, a pool of molecules with the dipoles oriented collinearly to the excitation light's electric vector will be preferentially excited, so that in the case of slow rotation, a relatively high anisotropy is expected. As the energy is transferred in a nonradiative manner from the initially excited molecules to other molecules, situated at different angles (except for 90 deg), the photons emitted will then be characterized with decreased anisotropy values.

Depicted on Fig. 5 is a comparison column chart showing the average intensity-weighted steady state anisotropy values measured from eGFP(wt), 97Q-eGFP(hsp104Δ), and 97Q-eGFP(wt). The value of 0.49 ± 0.03 obtained from the eGFP(wt) appeared to be not much lower than the maximal value of 0.57, available at two-photon excitation. This can be explained with a relatively long rotational correlation time for eGFP, so that it slightly affects its depolarization within the radiative decay time.[60] A strong depolarization was observed for the 97Q-eGFP(wt): an anisotropy value as low as 0.25 ± 0.02 was recorded. As the volume and molecular mass of the aggregates are much higher than that for the free fluorophore, the rotational depolarization can be ruled out, leading us to the conclusion that homo-FRET is the main cause for the phenomenon observed. A depolarization of eGFP fluorescence as a result of homo-FRET has been also demonstrated in earlier works.[61]

Contrary to expectations, 97Q-eGFP(hsp104Δ) exhibited a steady state anisotropy value of 0.44 ± 0.11, which was lower than the value observed for the eGFP(wt). This can be partly explained with some probability of aggregation even in the absence of the hsp104. Earlier works have demonstrated that in 10 to 40% of the hsp104Δ cells, the aggregates can still be found even in the absence of the chaperone.[12] Indeed, in some measurements, a strong depolarization was observed, with the anisotropy values similar to that of the aggregates.

3.4 *Cytotoxicity and Autofluorescence*

The data on the cytotoxicity of the polyQ aggregates in yeast is controversial. In the early studies, none or little toxicity was reported even for 103Q tracts—at most, there was just a slight

Table 1 Results of the proliferation assay for wt and hsp 104Δ cells with and without 97Q expression.

	2 h	4 h	8 h	12 h
pYES2(wt)	0.63±0.02	0.67±0.02	1.07±0.08	3.14±0.22
97Q(wt)	0.61±0.01	0.65±0.01	1.01±0.06	2.38±0.13
pYES2(hsp 104Δ)	0.62±0.02	0.67±0.02	1.03±0.07	2.98±0.25
97Q(hsp 104Δ)	0.60±0.02	0.64±0.02	1.02±0.02	2.57±0.11

Cells harboring empty vector pYES2, pYES2(wt), and pYES2(hsp 104Δ), were used as controls. The numbers are the density of the culture represented by the OD_{600} values.

reduction in final culture density.[8] Later studies, however, reported toxicity of expanded polyQ especially at the late stages after expression with the accumulation of the aggregated protein in the nucleus, leading to cell death with the markers, characteristic for apoptosis[62–64] [mitochondrial fragmentation, reactive oxygen species (ROS) accumulation, and caspases activation). The latter, in its turn, may result in the increased level of autofluorescence intensity and perturbations in the intracellular environment, and hence affect the eGFP fluorescence lifetime.[65,66]

To investigate the level of 97Q cytotoxicity in our experiment, cell proliferation of wt and hsp104Δ yeast cells was assessed during 12 h after the induction of 97Q by measuring the culture's optical density at 600 nm (OD_{600}). The results are presented in Table 1 and Fig. 6. The OD_{600} values for all the samples were identical within the first 8 h of observation. At the 12th hour, wt cells expressing 97Q exhibited decreased OD_{600} values as compared to the control cells (2.38 ± 0.13 versus 3.14 ± 0.22). For the same time point, a decrease was also observed for the hsp104Δ cells: expression of the 97Q resulted in the reduction of the OD_{600} values from 2.98 ± 0.25 to 2.57 ± 0.11.

The influence of the autofluorescence was checked on the wt and hsp104Δ cells with and without expression of the 97Q protein. For all samples, we obtained the value of mean fluorescence lifetime (τ_m) ~1.35 ns with the intensity less than 10% of that recorded from the samples with eGFP. As shown in Fig. 7, on the induction of 97Q the autofluorescence intensity increased. However, the increase was observed both for the wt and hsp104Δ cells. Moreover, the autofluorescence, recorded from the hsp104Δ cells expressing 97Q appeared somewhat higher than for the wt cells. Therefore, the autofluorescence perturbations could not account for the lifetime dynamics observed.

4 Discussion

The experiments conducted revealed a decrease of the eGFP fluorescence lifetime in fusion with 97Q by ~300 ps as compared to the eGFP alone. Preventing aggregation of the polyQ extended tract through the elimination of Hsp104 chaperone led to the reverse of the 97Q-eGFP's fluorescence lifetime with just slightly smaller values than that recorded from the free eGFP.

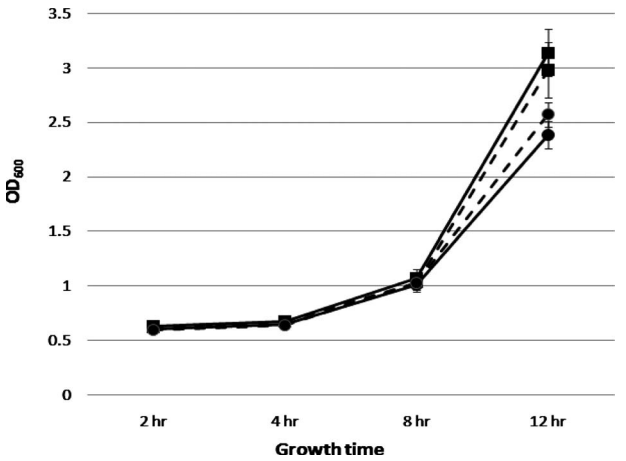

Fig. 6 Time-lapse measurement of cell growth after the induction of 97Q-eGFP. Cells harboring empty vector pYES2 did not express 97Q-eGFP and served as controls. No difference was observed for up to the 8th hour. In the 12th hour, a decrease in optical density was detected for both wt and hsp 104Δ cells expressing the 97Q (solid line with circle and dashed line with circles correspondingly) as compared to the control wt (solid line with squares) and hsp 104Δ cells (dashed line with squares).

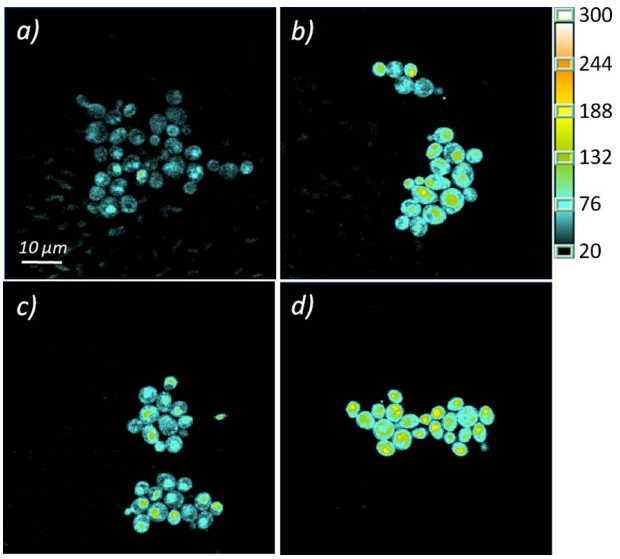

Fig. 7 Autofluorescence intensity of the samples: (a) wt cells, (b) hsp 104Δ cells, (c) wt cells expressing 97Q, and (d) hsp 104Δ expressing 97Q. The color bar is given in photons numbers. (Color online only.)

Table 2 Summary of the lifetime results for the measurements taken from 97Q-eGFP in wt and hsp 104Δ cells, as well as in their Ade2-proficient analogs.

	Cells			
Construct	wt	hsp 104Δ	wt Ade2	hsp 104Δ Ade2
eGFP	2.29±0.03 ns (9)	—	—	—
97Q-eGFP	2±0.06 ns (25)	2.24±0.03 ns (9)	2.07±0.02 ns (5)	2.24±0.02 ns (5)

Values are given as $\tau_m \pm$ standard deviation with the number of the data points in (n), representing the number of images analyzed.

The possibility of the direct nonradiative transfer of energy from eGFP to the 4-aminoimidazole ribotide and red Ade2 dye was assessed by comparing the lifetime values of 97Q-eGFP(wt) (with the fluorescent metabolites accumulated) and 97Q-eGFP(Ade2) (with the restored purine biosynthesis and thus lack of potential FRET acceptors accumulation). Only a slight difference between both cell types was observed with 2 ± 0.06 ns obtained from 97Q-eGFP(wt) and 2.07 ± 17 ns obtained from 97Q-eGFP(wt Ade2). The measurement results of 97Q-eGFP taken from Ade2-deficient and proficient hsp104Δ cells also appeared to be identical (Tables 2 and 3). The data obtained proves lack of nonradiative energy transfer, meaning lack of contribution by the metabolites to the observed fluorescence lifetime decrease.

The autophagy of abnormal proteins to lysosomes, which are known to have acidic pH in their lumen, was shown to be not effective in our experiments, since no signal of the eGFP was detected from the vacuole. Hence, the influence of low pH on the fluorescence lifetime dynamics can also be ruled out.

Cell proliferation assay revealed slightly lower OD_{600} in the 12th hour on the 97Q induction in wt cells as compared to the control cells without polyQ protein. Despite the fact that some cell growth inhibition was observed, the degree of its manifestation was much lower than that reported in earlier works, which reported apoptosis induction by polyQ aggregation.[64] Moreover, a reduction in the OD_{600} value was observed also for the hsp104Δ cells expressing 97Q, indicating that the reduction of the cell density was caused by the expression of exogenous 97Q rather than the protein aggregation. The results obtained enable us to conclude that at this level of cytotoxicity no massive changes in the intracellular environment took place and thus it could not be the major contributor to the eGFP fluorescence lifetime changes recorded.

The reasons for the autofluorescence intensity increase on 97Q expression are unclear. However, since the increase was recorded from both wt and hsp104Δ cells, it is clear that this also could not account for the observed fluorescence lifetime dynamics.

Reviewing all of the preceding, the decrease of the eGFP fluorescence lifetime can supposedly be attributed to the influence of the aggregation per se. Although the exact reason for the phenomenon observed requires further investigation, we suggest two possible hypotheses for the observed fluorescence lifetime dynamics: homo-FRET between eGFP molecules due to their tight packing in aggregates and changes in refractive index of the eGFP environment at aggregation.

The existence of homo-FRET was demonstrated by fluorescence anisotropy imaging. A strong depolarization in 97Q-eGFP(wt) is indicative of the eGFP molecules being in close proximity. Theoretically, homo-FRET does not affect the recorded fluorescence lifetime since the transfer time is negligible as compared to the time the molecules spend on the

Table 3 Distribution of the P values calculated by a single-tailed ANOVA test.

	eGFP (wt)	97Q-eGFP (wt)	97Q-eGFP (hsp 104Δ)	97Q-eGFP (wt Ade2)	97Q-eGFP (hsp 104Δ Ade2)
eGFP (wt)		9.01×10^{-23}	0.00031	1.9×10^{-12}	0.002923409
97Q-eGFP (wt)	9.01×10^{-23}		2.86×10^{-13}	0.021511	7.63975×10^{-10}
97Q-eGFP (hsp 104Δ)	0.00031	2.86×10^{-13}		2.54×10^{-08}	0.973337613
97Q-eGFP (wt Ade2)	1.9×10^{-12}	0.021511	2.54×10^{-08}		3.24459×10^{-07}
97Q-eGFP (hsp 104Δ Ade2)	0.002923	7.64×10^{-10}	0.973338	3.24×10^{-07}	

excited state levels, and the fluorescence properties of the acceptor are identical to those of the donor. However, in special cases a direct dependence of the CFP fluorescence lifetime on the presence of homo-FRET was demonstrated earlier even for dimers and was suggested to result from the chromophore structure.[55] In the same work, however, the experiments failed to work the same dependence with eGFP. Moreover, other works, exploring homo-FRET of eGFP showed no changes in the fluorophore's fluorescence lifetime values.[61] Nevertheless, we assume that in the case of the aggregates, an increase in the number of molecules in a volume unit could lead to the continuous transfers of the energy quantum, and such an energy trap could lead to the decrease of the recorded fluorescence lifetime. A similar effect has been also reported earlier in Ref. 56.

The relation between refractive index and fluorescence lifetime was defined in 1962 by Strickler and Berg:[67]

$$\frac{1}{\tau_0} = 2.88 \times 10^{-9} n^2 \frac{\int I(\nu) \mathrm{d}\nu}{\int I(\nu) \nu^{-3} \mathrm{d}\nu} \int \frac{\varepsilon(\nu)}{\nu} \mathrm{d}\nu, \qquad (4)$$

where τ_0 is the natural lifetime, I is the fluorescence emission, ε is the extinction coefficient, ν is the emission spectrum in wavenumbers, and n is the refractive index. Although the equation describes the dependence for the natural lifetime only, the applicability of the same model has been demonstrated in experiments. Thus, the dependence of the GFP fluorescence lifetime on the square of the refractive index in solution was demonstrated by Suhling et al.[24] In their experiment, increasing a solution's refractive index from 1.35 to 1.46 by changing the glycerol contents from 10 to 90%, resulted in a drop from 2.68 to 2.17 ns for the GFP fluorescence lifetime. This dependence was further utilized to sense the spatial variation of the refractive index in live cells, which was demonstrated by other methods to vary from 1.35 in the cytoplasm to 1.46 to 1.60 for the plasma membrane.[68–71] However, in the majority of these works, FLIM was applied to reveal the spatial heterogeneities mainly within plasma membrane.[72–74] A change of refractive index was also associated with the eGFP fluorescence lifetime decrease on fusion to other proteins;[73] such dependence could be the reason for lack of full restoration of the free eGFP lifetime in 97Q-eGFP(hsp104Δ) observed in our experiments.

Deviations from the quadratic dependence were also demonstrated in some cases.[75] This, in particular, may be applicable for the molecules bound to optically thin layers characterized with the refractive index values different from the homogenous medium surrounding the fluorophore. In this case, a decrease of the fluorescence lifetime may result from the reflections of the emitted fluorescence at the interface and interference of the reflected field and the excited state dipole.[73,76] In this case, the radiative rate of a fluorophore depends on the orientation of the transition moment of the molecule with respect to the interface. Given that current data describes the aggregates as enriched in β-sheet structures, this model may apply to the dynamics observed and explain the broadening of the histogram recorded from the 97Q-eGFP(wt).

The results obtained suggest that application of fluorescence spectroscopy techniques for the study of misfolded and, as a result, aggregated proteins require a careful approach and consideration of the changes in the used fluorophores photophysical properties, in particular, as demonstrated, the fluorescence lifetime. This is especially important for qualitative measurements, such as, for example, FRET, which is used for the calculation of intermolecular distance.

Acknowledgments

This work is generously supported by the National Science Council under Grants NSC 97-3112-B-010-006, NSC 97-2627-M-010-006, NSC 96-2112-M-010-001, NSC 94-2311-B-010-007, NSC95-2311-B-010-004, and NSC96-2311-B-010-001 and by the Ministry of Education under the "Aim for Top University" project.

References

1. F. Chiti and C. M. Dobson, "Protein misfolding, functional amyloid, and human disease," *Annu. Rev. Biochem.* **75**, 333–366 (2006).
2. P. S. Reddy and D. E. Housman, "The complex pathology of trinucleotide repeats," *Curr. Opin. Cell Biol.* **9**(3), 364–372 (1997).
3. K. Mitsui, H. Doi, and N. Nukina, "Proteomics of polyglutamine aggregates," *Methods Enzymol.* **412**, 63–76 (2006).
4. A. J. Williams and H. L. Paulson, "Polyglutamine neurodegeneration: protein misfolding revisited," *Trends Neurosci.* **31**(10), 521–528 (2008).
5. H. Y. Zoghbi and H. T. Orr, "Glutamine repeats and neurodegeneration," *Annu. Rev. Neurosci.* **23**, 217–247 (2000).
6. J. K. Cooper, G. Schilling, M. F. Peters, W. J. Herring, A. H. Sharp, Z. Kaminsky, J. Masone, F. A. Khan, M. Delanoy, D. R. Borchelt, V. L. Dawson, T. M. Dawson, and C. A. Ross, "Truncated N-terminal fragments of huntingtin with expanded glutamine repeats from nuclear and cytoplasmic aggregates in cell culture," *Hum. Mol. Genet.* **7**(5), 783–790 (1998).
7. S. H. Li and X. J. Li, "Aggregation of N-terminal huntingtin is dependent on the length of its glutamine repeats," *Hum. Mol. Genet.* **7**(5), 777–782 (1998).
8. S. Krobitsch and S. Lindquist, "Aggregation of huntingtin in yeast varies with the length of the polyglutamine expansion and the expression of chaperone proteins," *Proc. Natl. Acad. Sci. U.S.A.* **97**(4), 1589–1594 (2000).
9. G. Huntington's Disease Collaborative Research, "A novel gene containing a trinucleotide repeat that is expanded and unstable on Huntington's disease chromosomes," *Cell* **72**, 971–983 (1993).
10. A. J. Tobin and E. R. Signer, "Huntington's disease: the challenge for cell biologists," *Trends Cell Biol.* **10**, 531–536 (2000).
11. R. M. Bonelli, G. K. Wenning, "Pharmacological management of Huntington's disease: an evidence-based review," *Curr. Pharm. Des.* **12**(21), 2701–2720 (2006).
12. B. Meriin, X. Zhang, N. B. Miliaras, A. Kazantsev, Y. O. Chernoff, J. M. McCaffery, B. Wendland, and M. Y. Sherman, "Aggregation of expanded polyglutamine domain in yeast leads to defects in endocytosis," *Mol. Cell. Biol.* **23**(21), 7554–7565 (2003).
13. S. L. Crick, M. Jayaraman, C. Frieden, R. Wetzel, and R. V. Pappu, "Fluorescence correlation spectroscopy shows that monomeric polyglutamine molecules form collapsed structures in aqueous solutions," *Proc. Natl. Acad. Sci. U.S.A.* **103**(45), 16764 (2006).
14. Y. Takahashi, Y. Okamoto, H. A. Popiel, N. Fujikake, T. Toda, M. Kinjo, and Y. Nagai, "Detection of polyglutamine protein oligomers in cells by fluorescence correlation spectroscopy," *J. Biol. Chem.* **282**(33), 24039 (2007).
15. H. R. Brignull, F. E. Moore, S. J. Tang, and R. I. Morimoto, "Polyglutamine proteins at the pathogenic threshold display neuron-specific aggregation in a pan-neuronal Caenorhabditis elegans model," *J. Neurosci.* **26**(29), 7597–7606 (2006).
16. S. K. Pollitt, J. Pallos, J. Shao, U. A. Desai, A. A. Ma, L. M. Thompson, J. L. Marsh, and M. I. Diamond, "A rapid cellular FRET assay of polyglutamine aggregation identifies a novel inhibitor," *Neuron* **40**, 685–694 (2003).
17. R. S. Rajan, M. E. Illing, N. F. Bence, and R. P. Kopito, "Specificity in intracellular protein aggregation and inclusion body formation," *Proc. Natl. Acad. Sci. U.S.A.* **98**(23), 13060–13065 (2001).
18. A. Weiss, D. Abramowski, M. Bibel, R. Bodner, V. Chopra, M. Di-

Figlia, J. Fox, K. Kegel, C. Klein, S. Grueninger, S. Hersch, D. Housman, E. Régulier, H. D. Rosas, M. Stefani, S. Zeitlin, G. Bilbe, and P. Paganetti, "Single-step detection of mutant huntingtin in animal and human tissues: a bioassay for Huntington's disease," *Anal. Biochem.* **395**, 8–15 (2009).
19. T. Takahashi, S. Kikuchi, S. Katada, Y. Nagai, M. Nishizawa, and O. Onodera, "Soluble polyglutamine oligomers formed prior to inclusion body formation are cytotoxic," *Hum. Mol. Genet.* **17**(3), 345–356 (2008).
20. C. Behrends, C. A. Langer, R. Boteva, U. M. Böttcher, M. J. Stemp, G. Schaffar, B. V. Rao, A. Giese, H. Kretzschmar, K. Siegers, and F. U. Hartl, "Chaperonin TRiC promotes the assembly of polyQ expansion proteins into nontoxic oligomers," *Mol. Cell* **23**, 887–897 (2006).
21. W. Fecke, M. Gianfriddo, G. Gaviraghi, G. C. Terstappen, and F. Heitz, "Small molecule drug discovery for Huntington's disease," *Drug Discovery Today* **14**(9–10), 453–364 (2009).
22. S. S. Vogel, C. Thaler, and S. V. Koushik, "Fanciful FRET," *Sci. STKE* **2006**(331), 2–9 (2006).
23. B. Valeur, *Molecular Fluorescence: Principles and Applications*, Wiley, Weinheim, New York, Chichester, Brisbane, Singapore, Toronto (2001).
24. K. Suhling, K. Siegel, D. Phillips, P. M. W. French, S. Leveque-Fort, S. E. D. Webb, and D. M. Davis, "Imaging the environment of green fluorescent protein," *Biophys. J.* **83**, 3589–3595 (2002).
25. T. Nakabayashi, H. P. Wang, M. Kinjo, and N. Ohta, "Application of fluorescence lifetime imaging of enhanced green fluorescent protein to intracellular pH measurements," *Photochem. Photobiol. Sci.* **7**(6), 668–670 (2008).
26. A. Miyawaki, J. Llopis, R. Heim, J. M. McCaffery, J. A. Adams, M. Ikura, and R. Y. Tsien, "Fluorescent indicators for Ca^{2+} based on green fluorescent proteins and calmodulin," *Nature (London)* **388**, 882–887 (1997).
27. C. M. Dooley, T. M. Dore, G. T. Hanson, W. C. Jackson, S. J. Remington, and R. Y. Tsien, "Imaging dynamic redox changes in mammalian cells with green fluorescent protein indicators," *J. Biol. Chem.* **219**, 22284–22293 (2004).
28. A. Miyawaki, "Visualization of the spatial and temporal dynamics of intracellular signaling," *Dev. Cell* **4**(3), 295–305 (2003).
29. H. Wallrabe and A. Periasamy, "Imaging protein molecules using FRET and FLIM microscopy," *Curr. Opin. Biotechnol.* **16**(1), 19–27 (2005).
30. V. Calleja, S. M. Ameer-Beg, B. Vojnovic, R. Woscholski, J. Downward, and B. Larijani, "Monitoring conformational changes of proteins in cells by fluorescence lifetime imaging microscopy," *Biochem. J.* **372**, 33–40 (2003).
31. J. Klucken, T. F. Outeiro, P. Nguyen, P. J. McLean, and B. T. Hyman, "Detection of novel intracellular {alpha}-synuclein oligomeric species by fluorescence lifetime imaging," *FASEB J.* **20**(12), 2050−2057 (2006).
32. O. Berezovska, B. J. Bacskai, and B. T. Hyman, "Monitoring proteins in intact cells," *Sci. Aging Knowl. Environ.* **2003**(23), pe14 (2003).
33. V. N. Uversky, "Nanoimaging in protein-misfolding and-conformational diseases," *Nanomedicine* **2**(5), 615–643 (2007).
34. R. Y. Tsien, "The green fluorescent protein," *Annu. Rev. Biochem.* **67**, 509–544 (1998).
35. M. Zimmer, "Green fluorescent protein: applications, structure, and related photophysical behavior," *Chem. Rev. (Washington, D.C.)* **102**, 759–781 (2002).
36. W. Cody, D. C. Prasher, W. M. Westler, F. G. Prendergast, and W. W. Ward, "Chemical structure of the hexapeptide chromophore of the Aequorea green-fluorescent protein," *Biochemistry* **32**(5), 1212–1218 (1993).
37. H. Katayama, A. Yamamoto, N. Mizushima, T. Yoshimori, and A. Miyawaki, "GFP-like proteins stably accumulate in lysosomes," *Cell Struct. Funct* **33**, 1–12 (2008).
38. R. Heim, A. B. Cubitt, and R. Y. Tsien, "Improved green fluorescence," *Nature (London)* **373**(6516), 663–664 (1995).
39. T. T. Yang, L. Cheng, and S. R. Kain, "Optimized codon usage and chromophore mutations provide enhanced sensitivity with the green fluorescent protein," *Nucleic Acids Res.* **24**(22), 4592–4593 (1996).
40. A. B. Meriin, X. Zhang, X. He, G. P. Newnam, Y. O. Chernoff, and M. Y. Sherman, "Huntingtin toxicity in yeast model depends on polyglutamine aggregation mediated by a prion-like protein Rnq1," *J. Cell Biol.* **157**, 997–1004 (2002).
41. U. Guldener, S. Heck, T. Fielder, J. Beinhauer, and J. H. Hegemann, "A new efficient gene disruption cassette for repeated use in budding yeast," *Nucleic Acids Res.* **24**(13), 2519–2524 (1996).
42. W. Becker, *Advanced Time-Correlated Single Photon Counting Techniques*, Springer, Berlin, Heidelberg (2005).
43. L. S. Weisman, R. Bacallao, and W. Wickner, "Multiple methods of visualizing the yeast vacuole permit evaluation of its morphology and inheritance during the cell cycle," *J. Cell Biol.* **105**(4), 1539–1547 (1987).
44. P. J. Muchowski, G. Schaffar, A. Sittler, E. E. Wanker, M. K. Hayer-Hartl, and F. U. Hartl, "Hsp70 and hsp40 chaperones can inhibit self-assembly of polyglutamine proteins into amyloid-like fibrils," *Proc. Natl. Acad. Sci. U.S.A.* **97**, 7841–7846 (2000).
45. P. J. Muchowski, K. Ning, C. D'Souza-Schorey, and S. Fields, "Requirement of an intact microtubule cytoskeleton for aggregation and inclusion body formation by a mutant huntingtin fragment," *Proc. Natl. Acad. Sci. U.S.A.* **99**, 727–732 (2002).
46. T. Shimohata, A. Sato, J. R. Burke, W. J. Strittmatter, S. Tsuji, and O. Onodera, "Expanded polyglutamine stretches form an 'aggresome'," *Neurosci. Lett.* **323**, 215–218 (2002).
47. Y. P. Bao, L. J. Cook, D. O'Donovan, E. Uyama, and D. C. Rubinsztein, "Mammalian, yeast, bacterial, and chemical chaperones reduce aggregate formation and death in a cell model of oculopharyngeal muscular dystrophy," *J. Biol. Chem.* **277**(14), 12263–12269 (2002).
48. A. Wyttenbach, J. Carmichael, J. Swartz, R. A. Furlong, Y. Narain, J. Rankin, and D. C. Rubinsztein, "Effects of heat shock, heat shock protein 40 (HDJ-2), and proteasome inhibition on protein aggregation in cellular models of Huntington's disease," *Proc. Natl. Acad. Sci. U.S.A.* **97**(6), 2898–2903 (2000).
49. J. Shorter and S. Lindquist, "Hsp104 catalyzes formation and elimination of self-replicating Sup35 prion conformers," *Science* **304**,(5678), 1793–1797 (2004).
50. D. A. Hattendorf and S. L. Lindquist, "Cooperative kinetics of both Hsp104 ATPase domains and interdomain communication revealed by AAA sensor-1 mutants," *EMBO J.* **21**(1–2), 12–21 (2002).
51. E. W. Jones and G. R. Fink, "Regulation of amino acid and nucleotide biosynthesis in yeast," in *The Molecular Biology of the Yeast Saccharomyces: Metabolism and Gene Expression*, pp. 181–299, Cold Spring Harbor Laboratory, Cold Spring Harbor, NY (1982).
52. G. Moat, C. N. Wilkins, and H. Friedman, "A role for biotin in purine biosynthesis," *J. Biol. Chem.* **223**(2), 985–991 (1956).
53. A. Ciechanover, "Intracellular protein degradation: from a vague idea, through the lysosome and the ubiquitin-proteasome system, and onto human diseases and drug targeting (Nobel lecture)," *Angew. Chem.* **44**(37), 5944–5967 (2005).
54. B. Ravikumar, R. Duden, and D. C. Rubinsztein, "Aggregate-prone proteins with polyglutamine and polyalanine expansions are degraded by autophagy," *Hum. Mol. Genet.* **11**(9), 1107–1117 (2002).
55. S. V. Koushik and S. S. Vogel, "Energy migration alters the fluorescence lifetime of cerulean: implications for fluorescence lifetime imaging Forster resonance transfer measurements," *J. Biomed. Opt.* **13**(3), 031204 (2008).
56. R. Luchowski, E. G. Matveeva, I. Gryczynski, E. A. Terpetsching, L. Patsenker, G. Laczko, J. Borejdo, and Z. Gryczynski, "Single molecule studies of multiple fluorophore-labeled antibodies. Effect of Homo-FRET on the number of photons available before photobleaching," *Curr. Pharm. Biotechnol.* **9**, 411–420 (2008).
57. S. S. Vogel, C. Thaler, P. S. Blank, and S. Koushik, "Time-resolved fluorescence anisotropy," Chap. 10 in *FLIM Microscopy in Biology and Medicine*, A. Periasamy and R. M. Clegg, Eds., pp. 245–288, CRC Press, Boca Raton, FL (2009).
58. M. Tramier, T. Piolot, I. Gautier, V. Mignotte, J. Coppey, K. Kemnitz, C. Durieux, and M. Coppey-Moisan, "Homo-FRET versus hetero-FRET to probe homodimers in living cells," Chap. 25 in *Methods in Enzymology*, Vol. **360**, part A, G. Marriott and I. Parker, Eds., pp. 580–597, Academic Press, San Diego, CA (2003).
59. D. M. Jameson, J. C. Croney, and P. D. J. Moens, "Fluorescence: basic concepts, practical aspects, some anecdotes," Chap. 1 in *Methods in Enzymology*, Vol. **360**, part A, G. Marriott and I. Parker, Eds., pp. 1–44, Academic Press (2003).
60. S. T. Hess, E. D. Sheets, A. Wagenknecht-Wiesner, and A. Heikal, "Quantitative analysis of the fluorescence properties of intrinsically fluorescent proteins in living cells," *Biophys. J.* **85**, 2566–2580 (2003).

61. I. Gautier, M. Tramier, C. Durieux, J. Coppey, R. B. Pansu, J.-C. Nicolas, K. Kemnitz, and M. Coppey-Moisan, "Homo-FRET microscopy in living cells to measure monomer-dimer transition of GFP-tagged proteins," *Biophys. J.* **80**, 3000–3008 (2001).
62. J. P. Vonsattel and M. DiFiglia, "Huntington disease," *J. Neuropathol. Exp. Neurol.* **57**, 369–384 (1998).
63. T. de Cristofaro, A. Affaitati, A. Feliciello, E. V. Avvedimento, and S. Varrone, "Polyglutamine-mediated aggregation and cell death," *Biochem. Biophys. Res. Commun.* **272**, 816–821 (2000).
64. S. Sokolov, A. Pozniakovsky, N. Bocharova, D. Knorre, and F. Severin, "Expression of an expanded polyglutamine domain in yeast causes death with apoptotic markers," *Biochim. Biophys. Acta* **1757**, 660–666 (2006).
65. H. W. Wang, V. Gukassyan, C. T. Chen, Y. H. Wei, H. W. Guo, J. S. Yu, and F. J. Kao, "Differentiation of apoptosis from necrosis by dynamic changes of reduced nicotinamide adenine dinucleotide fluorescence lifetime in live cells," *J. Biomed. Opt.* **13**, 054011 (2008).
66. V. Ghukasyan, Y. Y. Hsu, S. H. Kung, and F. J. Kao, "Application of fluorescence resonance energy transfer resolved by fluorescence lifetime imaging microscopy for the detection of enterovirus 71 infection in cells," *J. Biomed. Opt.* **12**, 024016 (2007).
67. S. J. Strickler and R. A. Berg, "Relationship between absorption intensity and fluorescence lifetime of molecules," *J. Chem. Phys.* **37**, 814–822 (1962).
68. C. L. Curl, C. J. Bellair, T. Harris, B. E. Allman, P. J. Harris, A. G. Stewart, A. Roberts, K. A. Nugent, and L. M. D. Delbridge, "Refractive index measurement in viable cells using quantitative phase-amplitude microscopy and confocal microscopy," *Cytometry, Part A* **65A**, 88–92 (2005).
69. W. Choi, C. Fang-Yen, K. Badizadegan, S. Oh, N. Lue, R. R. Dasari, and M. S. Feld, "Tomographic phase microscopy," *Nat. Med.* **4**(9), 717–720 (2007).
70. S. Johnsen and E. A. Widder, "The physical basis of transparency in biological tissue: ultrastructure and the minimization of light scattering," *J. Theor. Biol.* **199**(2), 181–198 (1999).
71. J. Beuthan, O. Minet, J. Helfmann, M. Herrig, and G. Muller, "The spatial variation of the refractive index in biological cells," *Phys. Med. Biol.* **41**(3), 369–382 (1996).
72. B. Treanor, P. M. P. Lanigan, K. Suhling, T. Schreiber, I. Munro, M. A. A. Neil, D. Phillips, D. M. Davis, and P. M. W. French, "Imaging fluorescence lifetime heterogeneity applied to GFP-tagged MHC protein at an immunological synapse," *J. Microsc.* **217**(1), 36−43 (2005).
73. C. Tregidgo, J. A. Levitt, and K. Suhling, "Effect of refractive index on the fluorescence lifetime of green fluorescent protein," *J. Biomed. Opt.* **13**, 031218 (2008).
74. H. J. van Manen, P. Verkuijlen, P. Wittendorp, V. Subramaniam, T. K. van den Berg, D. Roos, and C. Otto, "Refractive index sensing of green fluorescent proteins in living cells using fluorescence lifetime imaging microscopy," *Biophys. J.* **94**(8), 67–69 (2008).
75. D. Toptygin, R. S. Savtchenko, N. D. Meadow, S. Roseman, and L. Brand, "Effect of the solvent refractive index on the excited-state lifetime of a single tryptophan residue in a protein," *J. Phys. Chem. B* **106**(14), 3724–3734 (2002).
76. M. M. G. Krishna and N. Periasamy, "Fluorescence of organic dyes in lipid membranes: site of solubilization and effects of viscosity and refractive index on lifetimes," *J. Fluoresc.* **8**(1), 81–91 (1998).